THE INTERPLAY BETWEEN FLEXURAL STRESSES AND MAGMA RESERVOIR DYNAMICS BENEATH LARGE VENUSIAN VOLCANOES. Gerald A. Galgana[1], Patrick J. McGovern[1], and Eric B. Grosfils[2]; [1]Lunar and Planetary Institute, USRA, 3600 Bay Area Blvd., Houston, TX 77058 (galgana@lpi.usra.edu, mcgovern@lpi.usra.edu); [2]Geology Department, Pomona College, Claremont, CA 91711 (egrosfils@pomona.edu).

Introduction: Large volcanic edifices on Venus, derived from sub-edifice magma chambers that provide the primary source of lava and other eruptible materials, influence the state of stress at depth by exerting a significant downward load on the lithosphere. As edifices grow, the resulting flexure generates high differential stress (σ_D) magnitudes, distributed in a characteristic "dipole" pattern, with horizontal extension in the lower lithosphere and compression in the upper lithosphere [e.g., 1]; the latter will tend to inhibit magma ascent to shallow depth via vertical dikes [2].

Both magma chamber pressurization/rupture and lithospheric flexure beneath large volcanic edifices have been analyzed extensively [e.g., 2-5]; however, the interaction between these processes remains unexplored. Here we use numerical experiments to evaluate how a flexural stress state influences the rupture characteristics of an inflating magma chamber, and explore the implications for edifice-related volcanism.

Models: We build axisymmetric elastic models of the Venusian lithosphere (r =900 km; T_e = 20, 40 km), loaded with large conical volcanoes near the center of model domains. The full effects of gravitational loading are incorporated via body forces, and "lithostatic" pre-stress is applied to all the models. We use material parameters for the Venusian lithosphere and overlying volcano corresponding to those adopted by [2]. A pressurized spherical magma chamber (r =1, 3 km) is embedded at the symmetry axis in each model. We vary the depth of the magma reservoirs, individually pressurize them to the point of failure, and solve for stresses (and deformation) along the magma chamber wall and within the lithosphere. Following [4], failure occurs when the magma chamber walls reach the tensile regime; use of realistic cohesion values (≤10 MPa) does not change our results appreciably.

Results: The lithosphere exhibits maximum deflections and stresses beneath the center of the edifice, where the maxima of differential stress ($\sigma_D = \sigma_E - \sigma_C$, i.e., principal extensional stress minus principal compressive stress) occur at the top and the bottom of lithosphere, separated by a low-stress neutral plane (Fig. 1). The lower lithosphere is characterized by horizontal principal extension, with $\sigma_E = \sigma_\theta$ (out of plane) and $\sigma_C = \sigma_Z$ (vertical). The upper lithosphere experiences horizontal principal compression, with $\sigma_C = \sigma_R$ (radial: this changes to σ_θ near $r \sim 30$ km) and $\sigma_E = \sigma_Z$. Increasing T_e from 20 to 40 km deepens the neutral plane and decreases σ_D but does not significantly change the orientations and geometries described above.

In the lower lithosphere, the failure criterion (at σ = 0) is first reached at the bottom of the r = 1 km magma chamber (h = -2 km), where chamber-tangential stress σ_T and out-of-plane stress σ_θ approach equal magnitude. Since generally $\sigma_\theta > \sigma_T$, we would expect ongoing chamber failure to manifest as downward propagating, radially oriented dikes. For T_e = 20 km (red curves in Fig. 2), the bottom is far closer to failure than the top, whereas for T_e = 40 km, the top is almost at failure when the bottom fractures. In the upper lithosphere (blue curves in Fig. 2), $\sigma_T > \sigma_\theta$, and the failure criterion is first satisfied near the center of the chamber (h = -1 km), predicting sill intrusions.

For chambers near the neutral plane (green curves in Fig. 2), first failure is similar to the upper lithosphere cases (σ_T fails first) but occurs even higher on the chamber, predicting formation of cone sheets inclined ~23° from the midsection (i.e., similar to that predicted by non-flexural models [e.g., 6]). However, where the models of [6] predict propagation of magma toward the surface, our models predict that far from the chamber, the cone sheets should roll into sills due to prevailing stress orientations (see Fig. 1). Furthermore, the highest failure on the chamber occurs for the thick lithosphere case, in contrast to the situation for upper lithosphere chambers.

Our results show that variations in the flexural stress state with depth help control the locations of first failure on magma chambers and subsequent intrusion geometries. Near the symmetry axis, the "differential tectonic" stress $\sigma_{DT} = \sigma_H - \sigma_Z$ (in-plane horizontal minus vertical stress, $|\sigma_{DT}| \sim \sigma_D$,). σ_{DT} is positive for a region in horizontal extension and negative for horizontal compression. For a surface-loaded flexural stress state beneath the load, σ_{DT} is increasingly extensional with increasing depth.

Discussion: Our models show that $\sigma_E = \sigma_\theta$ throughout the lower lithosphere (Fig. 1), a condition that favors radial dike formation. We thus argue that such dikes become the preferred means of magma ascent through the lower lithosphere. Reservoirs emplaced in this region of the lithosphere fail at the bottom, similar to unloaded, pressurized chambers

embedded in a half space under uniaxial stress conditions (where $\sigma_R = \sigma_Z/3$) [4]. Given the prevailing stress orientations in the lower lithosphere (where σ_{DT} is extensional), vertically oriented intrusions radial to the chamber would be formed at the reservoir margin (where σ_E is horizontal). However, magma chambers in this environment would be unstable, since rupture would force magma back down toward its source at greater depths.

In contrast, reservoirs situated in the upper lithosphere are stable since they can hold magma influx overpressures until the point of failure (near the chamber midsection). Here, σ_{DT} is increasingly compressional with decreasing depth, and $\sigma_Z \neq \sigma_E$. Sustained magma flow and growth of the predicted mid-section sills may tend to expand the chamber laterally, creating oblate ellipsoidal reservoirs. Further pressurization of oblate chambers reinforces the midsection failure trend [e.g., 5]. In this way, magma movement is turned from vertical (summit-emergent) to lateral; sustained growth in this mode may create a wide chamber or sill complex of significant volume that affects the topography and tectonics of the overlying edifice [e.g., 7]. Such a mechanism may account for the mid-flank circumferential fractures seen at Sapas Mons, previously attributed to a ~100-km-diameter magma chamber [8]. Furthermore, lithospheric stress changes from sustained sill intrusion may re-open ascent pathways to the surface [e.g., 7, 9], leading to a cyclical evolution of magmatic emplacement styles. Some pathways may originate on the margins of the chamber/sill complex, manifesting as flank eruption sites such as those as found at Sif Mons and Kunapipi Mons on Venus [10] or Kilauea volcano on Earth.

In the neutral plane, magma chamber response is more complex: first failure is predicted at a point between the chamber midsection and the crest, with $\sigma_T = \sigma_E$ (Fig. 2). In a thick lithosphere model, stress magnitudes along the reservoir wall vary only by 20 MPa, suggesting the potential for a complex intrusion history if unmodeled stress perturbations are in play. Here, the resulting intrusion style will be cone sheets, with a greater dip of ~36° from the midsection. Given the prevailing compressive state in the upper lithosphere (Fig. 1), ascending, propagating cone sheets should again rotate into sub-horizontal sill geometries. Mid-lithosphere chambers require greater overpressure to reach failure than upper lithosphere chambers; thus, magma may be stored for longer periods in the former, potentially affecting the chemistry of erupted lavas. The overall stress difference across the neutral plane chamber surface is much smaller than for the upper and lower lithosphere chambers. Thus. external influences (e.g. regional stresses, similar to that produced by rift zones at Ozza Mons and Gula Mons), may exert a greater influence on failure locations and intrusion styles at midsection chambers compared to those at other locations in the lithosphere [i.e., 4].

References: [1] McGovern, P. and S. Solomon (1993) *JGR* 98 (E12): 23,553-23,579. [2] McGovern, P. and S. Solomon (1998) *JGR,* 92, 103(E5):11,071-11,101. [3] Comer, R. et al.(1985) *Rev. Geophys.* 23 : 61-92. [4] Grosfils, E. (2007) *JVGR*, 166: 47-75. [5] Hurwitz, D. et al. (2009) *JVGR*, 188: 379-394. [6] Gudmundsson, A. (2006) *Earth Sci. Rev.*, 79(1-2): 1-31. [7] McGovern, P. et al. (2001) *JGR*, 106(E10): 23,769-23,809. [8] Keddie, S. and J. Head (1994) *EMP*, 65: 129-190. [9] McGovern, P. (2007) *GRL*, 34:23, L23305, doi:10.1029/2007 GL031305, 2007. [10] Stofan, E. et al. (2001) *Icarus*, 152(1):75-95.

Figures

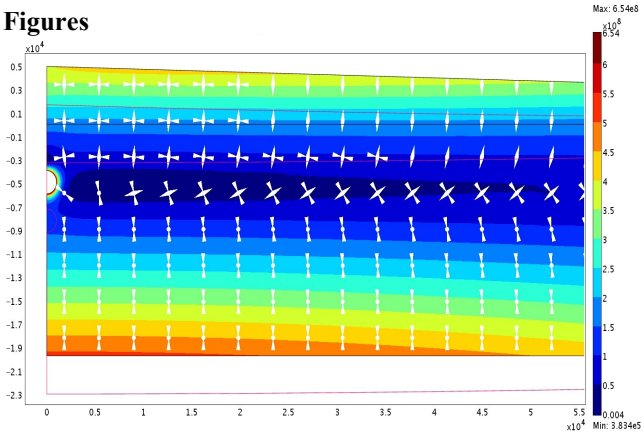

Figure 1. Section of axisymmetric model. T_e = 20 km, Depth to Center *DtC* = 5 km. Colors = σ_D (red = high, blue = low, units = Pa;); *x,y* axes in meters; Principal stress axes are shown by arrows (outwards = extension; inwards = compression; dots = out-of-plane). Deformed lithosphere is shown by the red outline.

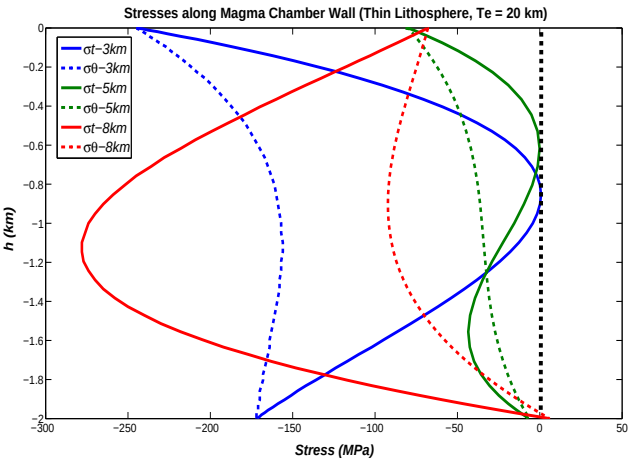

Figure 2. σ_T (red) and σ_θ (blue) along (spherical) magma chamber wall; Magma chambers situated on the upper lithosphere (T_e = 20 km, *DtC* =3 km) = blue curves; reservoirs at the lower lithosphere (*DtC* = 8 km) = red curves; at the neutral plane (*DtC* = 5 km) = green curves. Dashed black line = failure line.